Hard x-ray photoemission using standing-wave excitation applied to the MgO/Fe interface

Sven Döring, Frank Schönbohm, Ulf Berges, Reinert Schreiber, Daniel E. Bürgler, Claus M. Schneider, Mihaela Gorgoi, Franz Schäfers, Christian Papp, Benjamin Balke, Charles S. Fadley, and Carsten Westphal

Phys. Rev. B **83**, 165444 — Published 27 April 2011
DOI: 10.1103/PhysRevB.83.165444

BA11421

Hard x-ray photoemission studies using standing-wave excitation applied to the MgO/Fe interface

Sven Döring,[1,2,*] Frank Schönbohm,[1,2] Ulf Berges,[1,2] Reinert Schreiber,[3] Daniel E. Bürgler,[3] Claus M. Schneider,[3]
Mihaela Gorgoi,[4] Franz Schäfers,[4] Christian Papp,[5] Benjamin Balke,[5] Charles S. Fadley,[5,6] and Carsten Westphal[1,2]
[1]*Experimentelle Physik 1 - Technische Universität Dortmund, Otto-Hahn-Str. 4, D-44221 Dortmund, Germany*
[2]*DELTA - Technische Universität Dortmund, Maria-Goeppert-Mayer-Str. 2, D-44221 Dortmund, Germany*
[3]*Peter Grünberg Institut, PGI-6, Forschungszentrum Jülich GmbH, D-52425 Jülich, Germany*
[4]*Helmholtz-Zentrum Berlin für Materialien und Energie,*
Albert-Einstein-Str. 15, D-12489 Berlin, Germany
[5]*Materials Sciences Division, Lawrence Berkeley Laboratory,*
University of California, Berkeley, CA-94720, USA
[6]*Department of Physics, University of California at Davis, Davis, CA-95016, USA*
(Dated: February 9, 2011)

Many applications in electronics and spintronics rely on interfaces, which are buried a few nanometers deep and thus hardly accessible in real devices except for invasive techniques. Here, we report on hard x-ray photoemission spectroscopy combined with the x-ray standing-wave technique as a non-invasive method to access buried interfaces with a depth resolution of a few Å and enhanced interface sensitivity. Within these experiments, the film thicknesses and also the thicknesses of the intermixing layers are determined. We extend the data analysis scheme previously developed for soft x-rays to the hard x-ray regime and apply the method to buried epitaxial Fe/MgO interfaces, which play a crucial role in magnetic tunnel junctions and their applications. It was found that there was no detectable intermixing of reaction of the Fe and MgO layers at the interface.

PACS numbers: 68.49.Uv, 79.60.Jv, 79.60.Dp

I. INTRODUCTION

Thin layers with thicknesses in the range of a few nanometers and multilayers thereof feature new physical phenomena that are not present in bulk samples[1]. In many cases these phenomena crucially depend on the properties of the inevitable interfaces with the substrate and between individual layers. A prominent example is the tunneling magnetoresistance (TMR)[2,3] in magnetic tunnel junctions (MTJ), which is considered to be a key candidate for the development of real spintronic applications[1,4,5].

Largest TMR ratios have been reported for single-crystalline MgO(001) barriers in combination with Fe, CoFe, or CoFeB electrodes; in the case of CoFeB/MgO/CoFeB the values exceed 1000%[6]. The extremely large TMR effect in these MTJs is related to specific features of the band structures of MgO and Fe (or FeCo alloys). The MgO(001) barrier selects bands with a certain symmetry (Δ_1 bands) of the ferromagnetic electrodes that are highly spin-polarized at the Fermi level to contribute strongest to the tunneling current[7,8]. Other bands have a much lower tunneling probability or cannot couple to propagating states in the Fe electrodes. These effects only occur for coherent tunneling and thus require single-crystalline[9] or at least highly textured[10] MTJs. Detailed knowledge of the atomic interface properties, which govern the electronic properties, is therefore the key for understanding and optimizing the TMR effect. In fact, there are still fundamental open questions concerning the atomic structure at the interface[11–13]. The formation of an FeO interface layer, for instance, would significantly alter the electronic structure at the interface and impair the "symmetry filtering" of the MgO/Fe(001) interface.

However, interface properties of layered systems are difficult to investigate, because a specific interface layer constitutes only a tiny fraction of the complete structure and in addition is difficult to access if it is buried under other layers. One way to circumvent these difficulties are invasive techniques like secondary-ion mass spectroscopy (SIMS) or transmission electron microscopy (TEM). However, characteristic interface features could change when covering layers are altered or removed. The same objections apply when the interface is studied in an in-situ growth experiment in which the covering layers are missing that are essential for the device functionality. In previous studies of MgO/Fe interfaces[12,14], for instance, the MgO barrier was prepared in-situ by the evaporation of Mg in an O_2-rich atmosphere onto an Fe surface. The interface is thus close to the sample surface and within the information depth of photoemission spectroscopy (XPS), which is one of the most suitable methods to address questions about electronic properties and the chemical composition. However, for this preparation procedure the formation of iron oxide (FeO) at the interface is very likely. In contrast, technologically relevant MgO-based MTJs and most samples used to measure macroscopic properties such as the TMR effect are grown by evaporating or sputtering MgO as a compound, such that FeO formation is rather unlikely. In addition, postannealing of the complete multilayer stack is needed to obtain best properties, which inevitably means that the interface of interest is deeply buried inside the sample and not accessible with conventional XPS. Alternative characterization methods are rare and hard to find when the chemical composition, including oxidation states, is the subject of interest. Photoemission experiments mostly employ soft x-rays, which yield rather limited probing depths due to the short inelastic mean free path (IMFP) of the photoelectrons[27]. This fact clearly restricts the use of XPS in the soft x-ray regime for the investigation to deeply buried layers.

Very recently it has been shown that photoemission with several keV excitation energy, leading to high kinetic energies of the electrons, permits studying buried interfaces[16]. At kinetic energies above 1 keV the IMFP of photoelectrons rises above 20 Å and a probing depth of the same length-scale becomes possible[15]. Elastic scattering effects can be neglected here. Nevertheless, for these studies an enhanced depth resolution with high spectral resolution is desirable in order to investigate interface properties.

Enhanced depth resolution, on the other hand, can be obtained by exciting photoemission with an x-ray standing-wave field featuring a sinusoidally modulated electric field amplitude[17–19]. The high field amplitude in the maxima yields an enhanced sensitivity at the position (depth from the sample surface) of the maxima. Depth resolution results from shifting the field maxima through the sample by either varying the incidence angle around the Bragg angle (rocking curve) of a multilayer mirror or by laterally moving the x-ray beam along a wedge-shaped layer (wedge scan) grown on top of such a mirror[20]. In the latter case a field maximum can be shifted directly to the depth of the interface in order to increase the interface sensitivity as will be discussed below.

In this work we combine hard x-ray excitation with the standing-wave technique to perform photoemission spectroscopy of buried interfaces with high sensitivity and enhanced depth resolution. We study intermixing (due to roughness) and FeO formation at the interface between Fe and MgO layers. The experimental setup and the sample design are introduced in Sect. II. The data analysis of x-ray standing-wave field photoemission experiments in the soft x-ray regime was the subject of recent studies[21,22]. In Sect. III, we modify and extend the analytical approach to the high-energy range and test the influence of various model parameters on the simulated rocking curves to derive quantitative sensitivity and resolution values. In Sect. IV we present experimental rocking curves for various elements in our Fe/MgO samples and derive a set of model parameters that well describes all measurements. Enhanced interface sensitivity based on combining our simulations scheme and experimental data is demonstrated and discussed in detail in Sect. V. Our analysis of rocking curves and wedge scan reveals virtually no FeO formation at the interface, and there is only a minimal roughness-induced intermixing of the MgO and Fe layers. Thus, the growth process used for our samples results in a clean and sharp interface structure.

II. EXPERIMENTAL PROCEDURES

The Fe/MgO/Al layers are grown in a dedicated MBE system at the Research Center Jülich on a Si/MoSi$_2$ x-ray mirror provided by the Center for X-ray Optics at the LBNL. Afterwards the sample was transferred to the spectrometer at BESSY II storage ring of the Helmholtz-Zentrum Berlin für Materialien und Energie, where the measurements are performed without further treatment. Photoemission experiments were conducted at the HIKE experimental endstation[16,23] at the KMC-1 beamline that provides photon energies from 2 to 10 keV. Our measurements were done at $h\nu = 2010\,\mathrm{eV}$ and $h\nu = 4\,\mathrm{keV}$. The overall energy resolution of the instrument was tuned to approximately 200 meV. The divergence of the x-ray beam at the sample is found to be less than 6 mrad.

Figure 1 shows the geometry of the setup. The sample consists of a wedge-shaped Fe layer grown on an x-ray multilayer mirror (see Fig. 2). The spectrometer axis is perpendicular to the incoming beam. Thus, light with a grazing incidence angle leads to near-normal photoemission and therefore the highest probing depth and electron intensity. Sample rotation about the axis normal to the scattering plane (angle ϑ) permits recording of rocking curves. The vertical translation shifts the wedge through the x-ray beam, which is necessary to record wedge scans, i.e. measurements at different wedge thicknesses[20]. All rotations and translations are fully automated.

A standing-wave field with strong field modulation is created by the interference of the incoming x-ray beam and the x-rays reflected from the multilayer mirror that we used as a substrate[20]. High reflectivity is achieved for light incident at the first-order Bragg angle of the mirror, which in our case consisted of 80 double-layers of Si and MoSi$_2$ with individual thicknesses of 28.7 Å and 11.2 Å, respectively, yielding a multilayer periodicity of 39.9 Å. The angle of incidence for the first-order Bragg reflection is calculated to be $\vartheta = 2.3^\circ$ for $h\nu = 4\,\mathrm{keV}$[24], which leads to nearly normal photoemission at the HIKE experiment. This means that the photoelectrons entering the spectrometer leave the sample nearly perpendicular to the sample's surface, with an angle of 2.3° to the sample's surface normal. The Bragg reflection is less than 0.1° wide and has a reflectivity of $\sim 30\%$, from which we assume an effective interface roughness of 5 Å within the multilayer. An x-ray reflectivity measurement of our sample confirms an effective interface roughness of 5 Å or even less. A piece of the bare multilayer mirror that is used as a substrate in this work has previously been studied in detail with soft x-ray standing-wave photoemission experiments[22].

At the Bragg angle, the wave-length of the x-ray standing-wave field is independent of the wave-length of the incoming x-rays as discussed in Ref.[21]. At this angle the period of the standing-wave field is equal to the periodicity

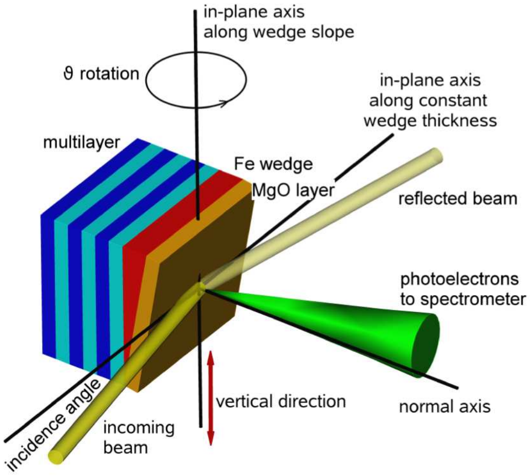

FIG. 1: Experimental geometry at the HIKE experimental endstation in relation to the wedge geometry of the sample. The vertical translation enables wedge scans and the rotation around the ϑ-axis is used for rocking curves.

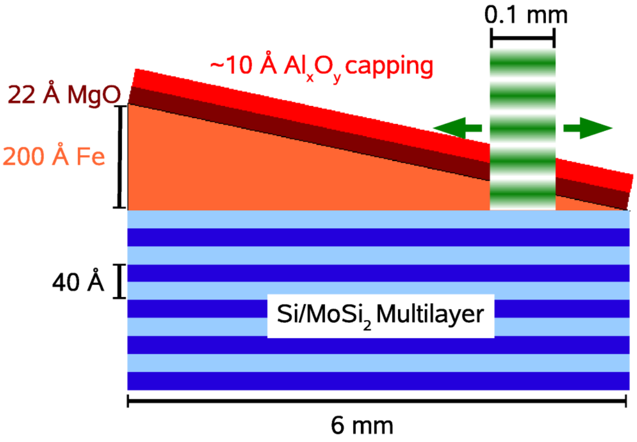

FIG. 2: Cross section of the sample consisting of the $Si/MoSi_2$ multilayer mirror, the Fe wedge, the MgO layer forming the Fe/MgO interface of interest, and the protective Al_xO_y capping. The residual oxide layer between the multilayer and the Fe wedge is not shown for clarity.

of the multilayer, which therefore defines the length scale and depth resolution of the experiment. In our experiment the multilayer periodicity is $\lambda \approx 40\,\text{Å}$. Therefore, the field intensity increases from minimum to maximum within $\lambda/4 \approx 10\,\text{Å}$. Conservatively assuming that we can resolve a tenth of the resulting photoemission intensity variation, we estimate the depth resolution to be about 1 Å.

The layers on top of the multilayer mirror were prepared by thermal evaporation after desorbing water and other contamination due to transfer through air by annealing the substate for 10 minutes at 100°C. Thus, a residual oxide on the topmost Si layer of the mirror was not removed. The Fe wedge with a nominal thickness varying from 0 to 200 Å over a width of 6 mm was covered by a layer of MgO with a constant thickness of nominally 20 Å. Finally, the sample was protected by a 10 Å-thick Al film, which upon air exposure converted into an Al_xO_y capping layer of slightly larger thickness. The Fe wedge was grown at 80°C and the other layers at room temperature. The thicknesses were monitored by quartz microbalances. Figure 2 shows schematically the sample structure together with the resulting x-ray standing-wave field.

The vertical translation indicated in Fig. 1 corresponds to a lateral motion of the x-ray beam with respect to the wedge in Fig. 2. Since the phase of the standing-wave is fixed relative to the multilayer mirror, a wedge scan results in a shifting of the Fe/MgO interface through four full periods over the whole wedge width of 6 mm. The beam diameter and thus the photoemitting area is small (around 100 μm) compared to the length of the wedge. Therefore, the wedge thickness can be assumed constant within the photoemitting area.

Figure 3 displays a survey spectrum of the sample measured at $h\nu = 4\,\text{keV}$. All major features of the spectrum

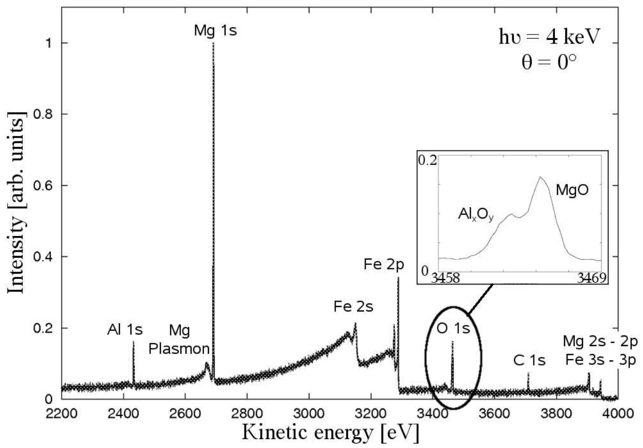

FIG. 3: Survey spectrum of the sample, measured at $h\nu = 4\,\mathrm{keV}$. The O 1s signal splits in two components due to chemical shifts as seen in spectra recorded at a higher resolution (inset). After a careful analysis of the wedge scans the two components were assigned to MgO and $\mathrm{Al}_x\mathrm{O}_y$, respectively.

can be assigned to core-level signals that were to be expected from the composition of the sample. The C 1s signal indicates surface contamination because the sample was exposed to ambient air during transport and transferred into the vacuum chamber without further cleaning.

For the standing-wave experiments we selected the strongest signals in the spectrum, namely Al 1s, Mg 1s, Fe 2p, and O 1s. All elements in the sample are represented by these four signals except the surface contamination. High-resolution spectra reveal that the O 1s signal is split into two components due to chemical shifts. These two signals are assigned to photoemission lines of oxygen in the MgO layer and in the $\mathrm{Al}_x\mathrm{O}_y$ capping layer.

III. ANALYTICAL ANALYSIS OF INTENSITY MODULATIONS IN HARD X-RAY STANDING-WAVE EXCITED PHOTOEMISSION EXPERIMENTS

In previous investigations[17,18,25] photoemission intensity modulations due to standing-wave excitation in the soft x-ray regime were studied. Here, we apply the photoelectron intensity modulation for high kinetic energies. In this case the IMFP is much larger than for soft x-rays, leading to a significantly larger probing depth. Due to the extension of the probing depth from a few Å to several nanometers, all parts of a thin film contribute more equally to the emitted signal, i.e. not only the parts close to the surface but also the deeply buried ones can contribute. In soft x-ray photoemission experiments the contribution from an intermixing zone that is a few Å thin below the layer under investigation which may be a few nanometers thick is very weak because it is strongly attenuated. Therefore, a recently developed analytical model for soft x-ray standing-waves neglects this contribution[22]. Only the intermixing zone on top of the layer can be reliably determined by soft x-ray photoemission experiments. In hard x-ray experiments the intermixing layer on the lower side of the film must be included into the calculations, too.

A. Model calculation

In order to develop a model describing the photoelectron intensity modulation for high electron kinetic energies we begin with the modulation of the XPS-intensity $I(\vartheta, h)$ resulting from the interference of the the incoming x-ray beam I_0 with its reflection $R(\vartheta) \cdot I_0$[26]

$$I(\vartheta, h) = I_0 \left[1 + R(\vartheta) + 2\sqrt{R(\vartheta)} \cos\left(\phi(\vartheta) - 2\pi \frac{h}{\lambda_{SW}} \right) \right], \tag{1}$$

where the intensity $I(\vartheta, h)$ is a function of the incidence angle ϑ and the position h of the considered emission center inside the standing-wave field with the period λ_{SW}. The reflectivity $R(\vartheta)$ and the phase between the incoming and reflected beams $\phi(\vartheta)$ are also functions of the incidence angle.

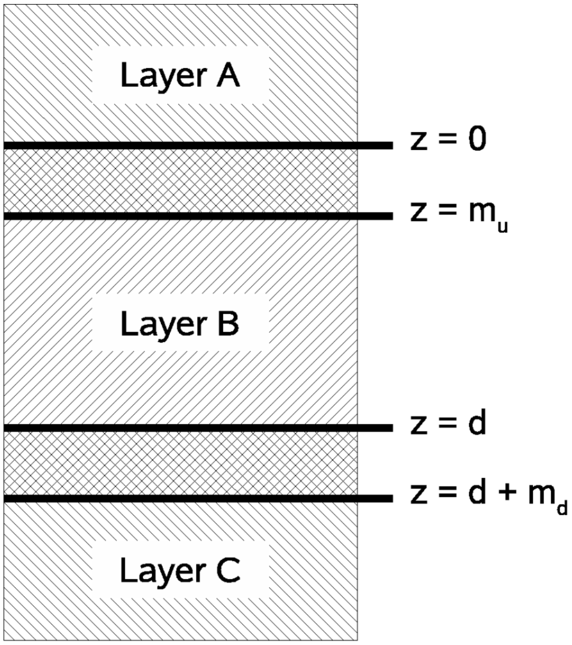

FIG. 4: Schematic drawing of the different layers and intermixing zones at the sample surface as assumed for the integration according to Eq. (2).

In the following, we will develop the formalism for the relative intensity $I_{rel} = I/I_0$ since experimental asymmetries are removed from this quantity while intensity modulation containing structure information is still preserved. The emission center in Eq. (1) is an infinitesimal thin layer only. Thus, in order to include layers with a given thickness of a real film we integrate over the z-direction:

$$I_{rel}(\vartheta, h, d, m_\mathrm{d}) = 1 + R(\vartheta) + 2\sqrt{R(\vartheta)}\frac{\int\limits_0^{d+m_\mathrm{d}} F(z)\cdot e^{-\frac{z}{\lambda_{IMFP}\cdot\sin(\alpha)}}\cos\left(\phi(\vartheta) - 2\pi\frac{h-z}{\lambda_{SW}}\right)dz}{\int\limits_0^{d+m_\mathrm{d}} F(z)\cdot e^{-\frac{z}{\lambda_{IMFP}\cdot\sin(\alpha)}}dz}, \tag{2}$$

where the integrals run over a film thickness from 0 to $d + m_\mathrm{d}$, and the function $F(z)$ represents weighting factors, which have to be applied in the different ranges of the integrals. They represent linear concentration profiles in the intermixing zones. The parameter d represents the thickness of the layer under investigation while the parameter m_d stands for the thickness of the intermixing zone below this layer. The attenuation of the photoemission signal is taken into account by the term $e^{-\frac{z}{\lambda_{IMFP}\cdot\sin(\alpha)}}$ with the parameters that represent the inelastic mean free path λ_{IMFP} and the angle α between the path of the photoelectron and the normal emission direction. Elastic scattering effects can be neglected here.

Figure 4 shows schematically the sample structure consisting of layers A, B, and C and intermixing zones between A and B, and B and C. Also, the upper and lower limits of integration are inserted in Eq. (2) as shown in Fig. 4: The full layer depth is given by parameter d with the thickness of the intermixing zones being m_u and m_d. The upper intermixing zone m_u is formally included into the layer B with thickness d, while the lower intermixing zone m_d is part of the layer C below. In this description the lower intermixing zone of a layer always reaches into the layer below. Thus, the sum over all layers' thicknesses d results in the total thickness of the sample.

The weighting function $F(z)$ has the form

$$F(z) = \begin{cases} \frac{z}{m_\mathrm{u}} & \text{for } 0 \leq z \leq m_\mathrm{u} \\ 1 & \text{for } m_\mathrm{u} \leq z \leq d \\ \frac{d+m_\mathrm{d}-z}{m_\mathrm{d}} & \text{for } d \leq z \leq d + m_\mathrm{d}. \end{cases} \tag{3}$$

The integrals for the first two ranges $0 \leq z \leq m_\mathrm{u}$ and $m_\mathrm{u} \leq z \leq d$ were solved[22] for the analysis of soft x-ray data. The third term can be rewritten in two parts, which are already known, too,

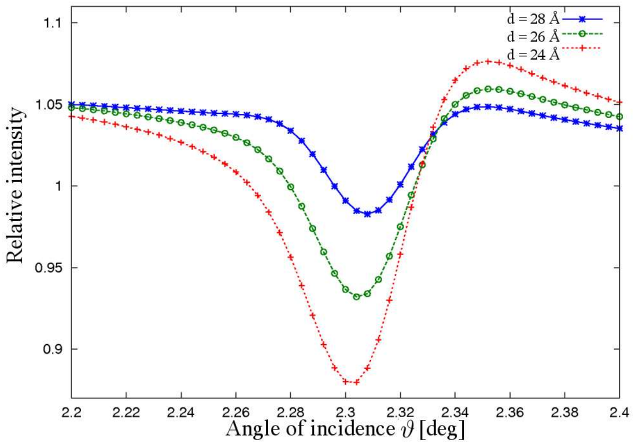

FIG. 5: Effect of MgO thickness on rocking curves of Mg 1s. The Fe thickness was fixed at 50 Å. The photon energy was 4 keV. A rather small variation of the layer thickness leads to a significant change of shape in the rocking curves.

$$\int_{d}^{d+m_\mathrm{d}} \frac{d+m_\mathrm{d}-z}{m_\mathrm{d}} f(z)dz = \frac{d+m_\mathrm{d}}{m_\mathrm{d}} \int_{d}^{d+m_\mathrm{d}} f(z)dz - \int_{d}^{d+m_\mathrm{d}} \frac{z}{m_\mathrm{d}} f(z)dz. \tag{4}$$

Thus, for an arbitrary function $f(z)$ (i.e., the attenuation of the photoemission signal or the product of the attenuation and the phase factor as shown in Eq. (2)) the relative intensity can easily be calculated by solving the integrals for the intermixing zones according to Eq. (4).

The influence of the divergence of the incoming x-ray beam on the intensity modulation was included into the calculation by a convolution of the calculated rocking curve with an Gaussian of 0.6 mrad FWHM according to the beam properties at the KMC-1 beamline [23].

B. Influence of the parameters

Before applying Eqs. (2) to (4) to experimental data, the influence of the main parameters on the resulting rocking curves is discussed by calculating several rocking curves as shown in Figs. 5, 6, and 7. The model parameters are chosen close to the experimental sample and setup. The x-ray energy was set to $h\nu = 4\,\mathrm{keV}$, with a $\lambda_{IMFP} = 47.5\,\text{Å}$ for the IMFP, calculated using the TPP-2M formula[27] for photoelectrons originating from the Mg 1s orbital in MgO excited by $h\nu = 4\,\mathrm{keV}$. The experimentally determined thickness and roughness parameters of the multilayer were used to calculate the reflectivity and the phase between incoming and reflected beams.

Figure 5 shows the influence of the MgO layer thickness on the shape and amplitude of the rocking curves. Only the layer thickness was varied in small steps of 2 Å, leading to a strong variation of the the rocking curves. The hard x-ray standing-wave experiment is obviously very sensitive to the thickness of the layers and the determination of the thickness is supposed to be accurate within one Å.

The influence of the thickness of the intermixing zones between MgO/Fe and $\mathrm{Al}_x\mathrm{O}_y$/MgO layers is shown in Fig. 6. The three rocking curves represent the intensity of the Mg 1s signal originating from a 28 Å thick MgO layer for different thicknesses of the mixing zones on both sides of the MgO layer ($\mathrm{m}_u = \mathrm{m}_d = \mathrm{m}$). Again, the influence on the general shape of the rocking curve is strong. The maximum of the relative intensity shifts from below the Bragg angle for a large mixing to above the Bragg angle in case of no intermixing. Although the layer thickness has a stronger influence on the shape of the rocking curve than the intermixing zone thickness, the latter can be determined with an accuracy of a few Å.

Finally, Fig. 7 shows the influence of inserting an intermixing zone below the MgO layer on the rocking curve simulation of hard x-ray data. If an intermixing zone between MgO and Fe is included, a much deeper minimum in the rocking curve is obtained. Obviously, the intermixing below the layer has a strong influence on the shape of the rocking curve in case of hard x-ray data with a larger IMFP and can no longer be neglected as is the case for soft x-rays.

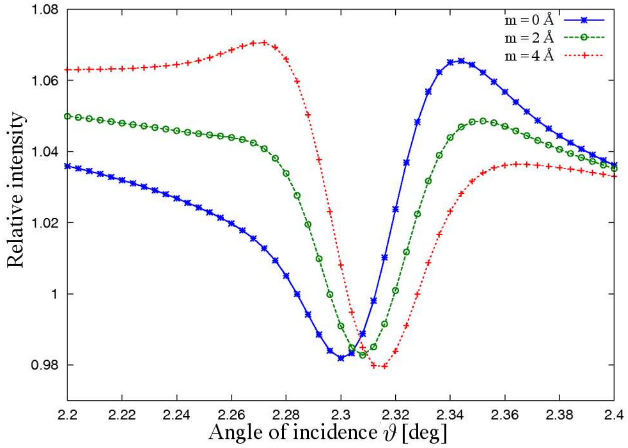

FIG. 6: Effect of MgO/Fe and Al$_x$O$_y$/MgO interface mixing on Mg 1s rocking curves. Here m$_u$ = m$_d$ = m. The Fe thickness was fixed at 50 Å. The photon energy was 4 keV. The general form of the rocking curve is very sensitive to the width of the intermixing zones.

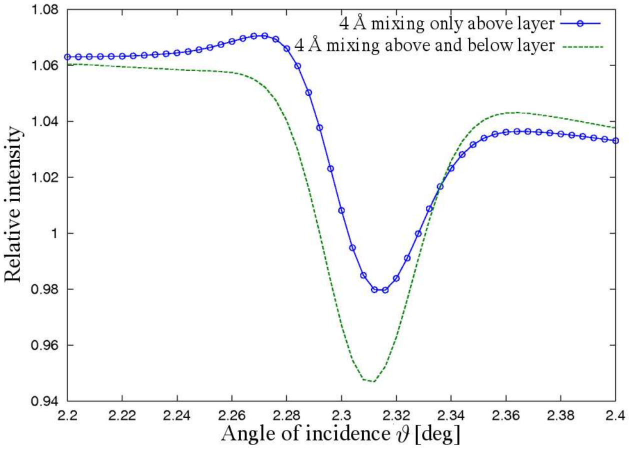

FIG. 7: Effect of a mixing zone m$_d$ between MgO and Fe. The Fe thickness was fixed at 50 Å. m$_u$ was set to 4 Å, while m$_d$ was 0 or 4 Å. The photon energy was 4 keV.

For a determination of the thickness of the intermixing zones and individual layers, the experimental curves $I_{Exp}(\vartheta)$ are compared to simulated rocking curves $I_{Sim}(\vartheta)$. The shape and amplitude of the calculated rocking curve strongly depends on even small changes of the structural parameters. For a quantitative comparison between experimental and simulated rocking curves, the structure search was carried out by varying the model parameters within an R-factor analysis, where the reliability factor R is defined as[28]:

$$R = \sum_{\vartheta} \frac{\left(I_{Sim}(\vartheta) - I_{Exp}(\vartheta)\right)^2}{I^2_{Sim}(\vartheta) + I^2_{Exp}(\vartheta)} \tag{5}$$

A perfect agreement between simulated and experimental rocking curves results in an R-factor of 0, while an R-factor of 1 means that there is no common feature between experimental and simulated rocking curves. During the R-factor analysis, we varied the thickness of the actual layer and of the intermixing zones above and below, beginning with the deepest-buried film and for each layer separately. The parameters are varied one by one and for each variation the R-factor was calculated. The range of precision for each parameter is the range over which the R-factor changes by less than 10%.

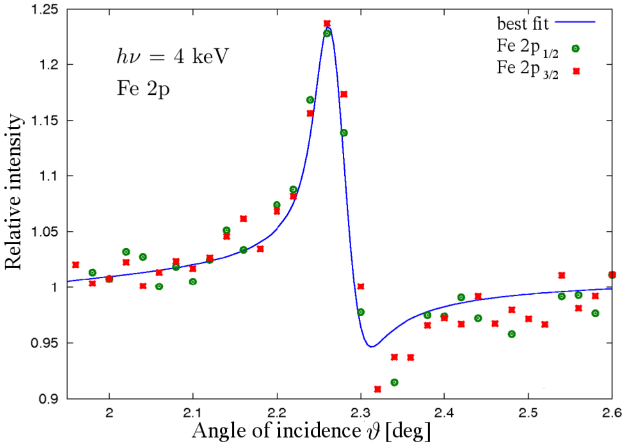

FIG. 8: Rocking curve of the Fe 2p$_{1/2}$ and Fe 2p$_{3/2}$ signals. The experimental data (dots and squares) are compared to the simulated results obtained for the best fit (solid line). In the optimized simulation we assumed a thickness of the Fe layer of d=32 Å with an interface intermixing thickness of m=m$_u$=m$_d$=1 Å.

Layer	Thickness of intermixing layer above film (m$_u$)	Film thickness (d)	Thickness of intermixing layer below film (m$_d$)
Al$_x$O$_y$ capping layer	6 Å	10 Å	6 Å
MgO layer	6 Å	28 Å	6 Å
Fe wedge (at rocking curve position)	1 Å	32 Å	1 Å
SiO$_2$ on top of the mirror	1 Å	10 Å	1 Å

TABLE I: Parameters of the sample as determined from the experiments. Each thickness includes the thickness of the intermixing layer on top of the layer according to Fig. 4.

IV. SCANNING THE ANGLE: ROCKING CURVES

Most of the rocking curves were recorded at a photon energy of $h\nu = 4\,\text{keV}$ in an angular range between $\vartheta = 1.9°$ and 2.7°, with an angle increment of 0.02°. Thus, every rocking curve consists of 41 single spectra. These spectra were fitted with appropriate line shapes (an asymmetric Voigt function with a Shirley inelastic background) in order to determine the intensities of the core-level signals to obtain $I_{Exp}(\vartheta)$.

Figure 8 shows the rocking curve of the Fe 2p spectrum, which is split into the Fe 2p$_{1/2}$ and Fe 2p$_{3/2}$ components due to spin-orbit coupling. Both components show very similar rocking curves, as expected. For the calculations of the Fe rocking curve, the thickness of the residual oxide layer directly on the multilayer mirror, the thickness d of the Fe layer, and the width of the intermixing zones above m$_u$ and below m$_d$ the Fe layer were varied, while all other parameters were kept constant. The nominal thickness of the Fe layer according to the position of the beam on the wedge is 35±3 Å.

The R-factor analysis was performed separately for the Fe 2p$_{1/2}$ and Fe 2p$_{3/2}$ sublevels yielding R = 0.026 and R = 0.019, respectively. In both cases the same set of parameters was obtained, d=32 Å and m=m$_u$=m$_d$=1 Å. Even though m$_u$ and m$_d$ were treated independently, we always found best agreement for m$_u$=m$_d$=m. The thickness of the Fe layer is in excellent agreement with the nominal thickness. The thickness of the residual oxide layer on the multilayer mirror was determined to be 10 Å in excellent agreement with previous results[22]. All optimized parameter are compiled in Table I. The 10% criterion of the R-factor analysis yields 1 Å and 3 Å for the precision of the film thickness and intermixing layer determinations, respectively.

In the next step, the analysis of the Mg 1s rocking curve was carried out following the same procedure as for Fe 2p (Fig. 9). Here, the thickness of the MgO layer and the thickness of the intermixing layers were varied as free parameters only, and the thickness of the Fe layer was kept constant. The smallest R-factor was achieved for a thickness of $d_{Mg} = 28\,\text{Å}$ with an intermixing layer thickness of m=6 Å. A similar analysis for the Al 1s data yields for the Al$_x$O$_y$ capping layer $d_{Al} = 10\,\text{Å}$ with an intermixing layer thickness of m=6 Å.

The oxygen signal in our spectra originates from two different parts of the sample, namely the MgO layer and the Al$_x$O$_y$ capping layer. The two components can easily be separated due to their different chemical shifts (inset

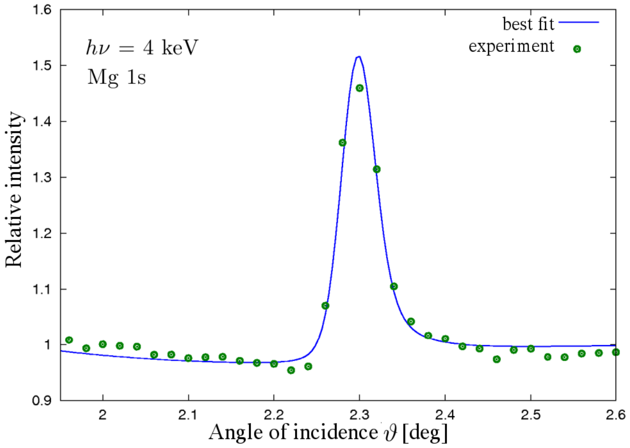

FIG. 9: Rocking curve of the Mg 1s signal, measured at $h\nu = 4\,\mathrm{keV}$. The experimental data (dots) are compared to the simulated results obtained for the best fit (solid line). In the optimized simulation for the Mg 1s signal we assumed a thickness of the MgO layer of 28 Å with m=6 Å.

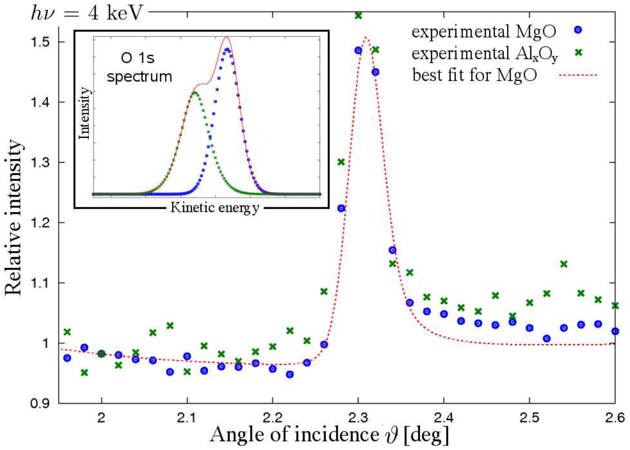

FIG. 10: Rocking curves of the two O 1s components that can be assigned to the MgO and Al_xO_y layers. The experimental data for the MgO component (dots) are compared to the simulated results obtained for the best fit (solid line). In the optimized simulation we assumed a thickness of the MgO layer of 28 Å with a thickness of the interface intermixing of m=6 Å. The inset shows the separation of the O 1s components due to MgO and Al_xO_y. The latter rocking curve is not shown for clarity.

of Fig. 10). Figure 10 shows the result of an R-factor analysis of the O 1s signal from the MgO layer. As a strong confirmation of the results discussed above in Fig. 9 for the Mg rocking curve, the smallest R-factor was found for the same set of parameters (Table I). This agreement confirms the consistency of our model because both rocking curves originate from atoms that are located in the same layer of the sample.

In order to further cross-check the results of the measurements performed at $h\nu = 4\,\mathrm{keV}$, the beamline was tuned to $h\nu = 2\,\mathrm{keV}$ to repeat all rocking curve measurements. During the change of the photon energy to $h\nu = 2\,\mathrm{keV}$ the illuminated spot on the sample stayed at the same position as for the rocking curves at 4 keV. The angular range was adjusted to the new Bragg angle and the spectra were taken for $\vartheta = 4.1°$ to $5.0°$. At the photon energy of $h\nu = 2\,\mathrm{keV}$, the Bragg reflection is broadened and therefore the stepsize was increased to $0.025°$.

The whole set of rocking curves was analyzed in the same manner as for the 4 keV data set, and we obtain within the experimental uncertainty the same results. As an example, Fig. 11 shows a typical experimental rocking curve for the Mg 1s signal and the best simulation as a solid line.

Note, that the second set of rocking curves at $h\nu = 2\,\mathrm{keV}$ is an independent data set to the data recorded at $h\nu = 4\,\mathrm{keV}$: a lower photon energy results in a decreased IMFP of the photoelectrons and the optical properties of the elements in the sample are different, too. Thus, the phase $\Phi(\vartheta)$ between incoming and reflected beam is altered , which significantly changes the shape of the rocking curves (compare Figs. 9 and 11). Nevertheless, the analysis of the

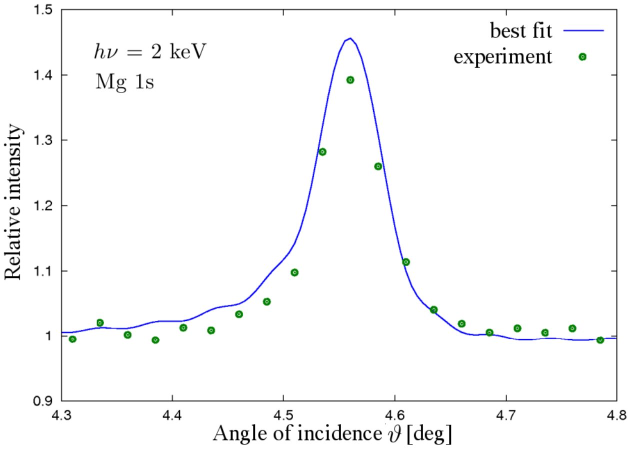

FIG. 11: Rocking curve of Mg 1s measured at $h\nu = 2$ keV. The dots represent the measured data and the line shows the best fit.

data set recorded at $h\nu = 2$ keV yields the same values for all film thicknesses and all thicknesses of of the intermixing regions.

V. SCANNING THE SAMPLE POSITION: WEDGE SCANS

In order to further confirm the rocking curve analysis and search for additional weak interface components such as possible formation of interfacial FeO, wedge scans across the sample surface were performed. For the measurement of wedge scans, the incidence angle of the x-rays was tuned to the first-order Bragg angle in order to obtain a strong standing-wave field with a high signal-to-noise ratio. The Bragg angle was precisely determined from the rocking curve experiments.

Spectra of the Al 1s, Mg 1s, Fe 2p, and O 1s core-level signals were measured as a function of the sample position relative to the beam by moving the sample perpendicular to the plane of incidence as indicated in Fig. 1. A stepsize of 0.1 mm was used to cover the sample length of 6 mm corresponding to $\sim$3 Å Fe thickness increments and leading to 61 spectra in total.

Figure 12 shows a full oscillation of the XPS signal due to a variation of the Fe layer thickness of 45 Å, which translates into a shifting of the Fe/MgO interface relative to the standing-wave by the same amount. All experimental data are plotted as relative intensities. The Fe $2\mathrm{p}_{1/2}$ and Fe $2\mathrm{p}_{3/2}$ intensities are plotted separately. For the O 1s intensity the component assigned to MgO was plotted. There is practically no difference between the wedge scans of the Mg 1s and O 1s signals because both signals originate from the same layer. Thus, their photoemission signal excited by the x-ray standing-wave must show an identical modulation as a function of the Fe thickness given by the sample position.

Rocking curves of all shown signals were calculated in order to simulate the wedge scan experiment. In this simulation, the only free parameter was the local thickness of the Fe-wedge, which changes with every step. The thickness and intermixing values derived from the rocking curve data (Table I) were kept constant.

Depth information can be extracted from the relative phase between the Fe- and MgO-sine functions as well as from the strength of the modulation. The experimental challenge is that the strength of the photoemission intensity modulation is directly connected to the x-ray reflectivity and thus strongly depends on the angle of incidence. A small angular variation causes a strong variation in the reflectivity if the Bragg reflection peak is as narrow as in this experiment. Therefore, we emphasized the matching of the relative phase more than the strength of the modulation.

In the next step of our analysis, the existence of a possible FeO interface layer was investigated. The wedge scan data can be used as a probe with increased interface sensitivity compared to simple XPS spectra. We select two spectra from the wedge scan data that have a maximum or a minimum of the standing-wave field at the interface. The difference between these two spectra emphasizes the interface contribution, while the bulk component is suppressed. As an example we look at the oxidation states of Fe at the interface, which would result in a chemically shifted component of the Fe 2p signal. The shifted component is supposed to be rather weak compared to the Fe 2p bulk signal because it originates from a thin layer at the interface if at all.

The location of each interface within the sample is well-known from the previous analysis of the rocking curves,

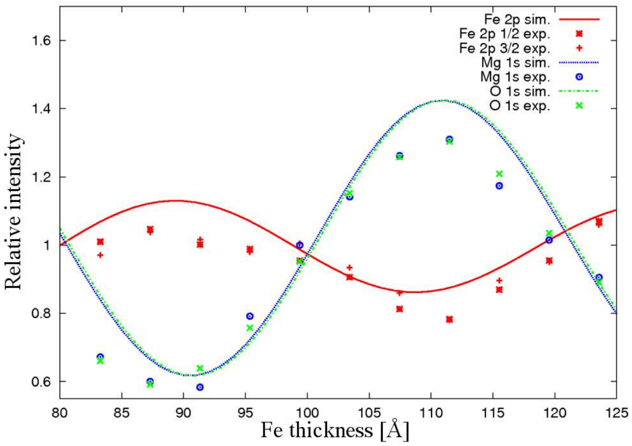

FIG. 12: Wedge scans measured at $h\nu = 4\,\mathrm{keV}$ for various elements originating from different layers of the sample. The markers represent the measured data and the lines show the calculations. The parameters that were obtained from the analysis of the rocking curves (Table I) were used for this simulation.

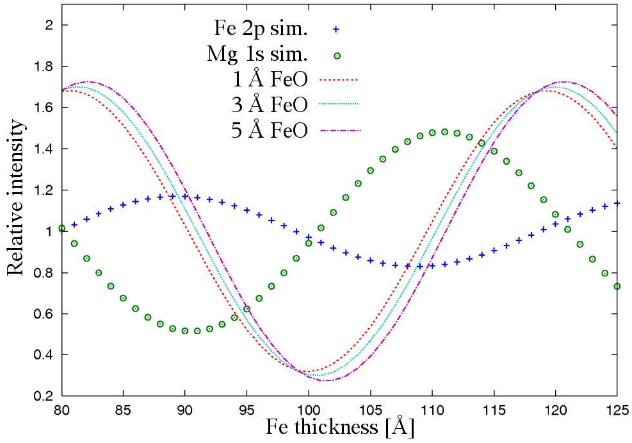

FIG. 13: Simulated wedge scans for assumed FeO layers of different thicknesses compared to optimized simulations for Fe 2p and Mg 1s. The positions of the minima and maxima for FeO hardly change, while the modulation of the intensity from the FeO layer is very strong in these cases.

as discussed in Figs. 8 to 11. Thus, a simulation of a wedge scan becomes possible and is displayed in Fig. 13. We assume FeO layers of different thicknesses and calculate the wedge scan modulation. A possible FeO interface layer must be thin, as proven by the analysis of the rocking curves. A layer that is more than a few Å thick would result in a lack of consistency in the model.

The modulation turns out to be rather strong and the positions of maxima and minima do not strongly shift with the FeO thickness. A high intensity can always be found at a wedge thickness of $\sim 80\,\text{Å}$ and a weak intensity at $\sim 100\,\text{Å}$. The difference between spectra measured at these Fe thicknesses is therfore very sensitive to the existence of an FeO layer.

The difference spectrum in Fig. 14 shows weakly decreased intensity slightly to the lower binding energy side of the Fe $2p_{3/2}$ component only. This feature is not likely to originate from an FeO layer because the chemical shift is expected (i) to be larger by about 2 eV, (ii) to lead to a higher binding energy, and (iii) to occur for the Fe $2p_{1/2}$ component, too[12]. The dip is located at the steepest gradient in the spectra, where statistical errors due to taking the difference of large numbers are substantial.

Further simulations show that any oxide component that is at least 3% of the bulk-component or stronger becomes clearly visible in the difference spectrum. Thus, it can be concluded that there is virtually no FeO present at the MgO/Fe interface, certainly not as a complete FeO layer.

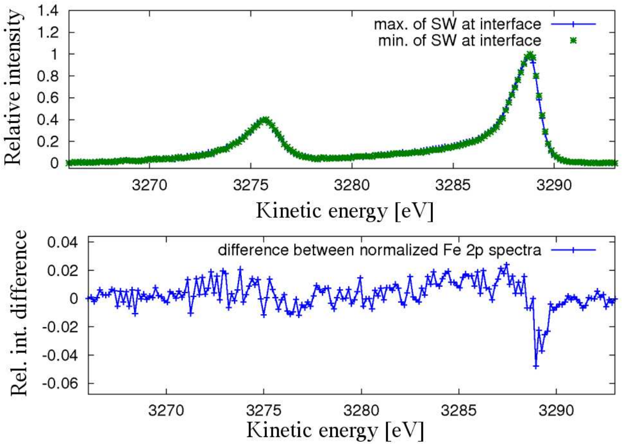

FIG. 14: Experimental spectra with a low and high standing-wave intensity at the MgO/Fe interface are compared in the upper part of the Figure. The difference of these spectra in the lower part is sensitive to interfacial FeO contributions.

VI. SUMMARY

We have combined hard x-rays and standing-wave excitation to perform photoemission of a interface that is buried a few nanomters deep. This combination opens the door to studying chemical composition and chemical binding states of atoms at a deeply buried interface.

The existing standard setup at the HIKE-experiment at BESSY II in combination with a dedicated sample structure including an x-ray mirror and a wedge-shaped layer enables this experimental technique. The analytical approach for the analysis of the photoemission data recorded with x-ray standing-waves was extended to account for the larger inelastic mean free path of photoelectrons excited by hard x-rays. The extended model permits simulating rocking curves and wedge scans in order to study the influence of structural parameters such as the layer thickness and the intermixing layer thickness. These parameters can be extracted with high precision from experimental data by performing an R-factor analysis.

We apply this novel method to the MgO/Fe interface of a sample grown by thermal evaporation of Fe and MgO. We find excellent agreement between the experimental data and the simulations for two independent data sets recorded at $h\nu = 4\,\mathrm{keV}$ and $h\nu = 2\,\mathrm{keV}$. In both cases, agreement is achieved for the same set of model parameters (Table I). The roughness-induced intermixing at the Fe/MgO interface is found to be $\sim 6\,\mathrm{Å}$. The formation of an interfacial FeO layer is excluded based on the newly developed procedure employing a difference spectrum with increased sensitivity for weak interface components. Thus, we showed that band-structure models which assume a thin layer of FeO at the MgO/Fe interface cannot be applied to all samples and TMR-devices in general.

To our knowledge, this is the first successful attempt to explore the deeply buried MgO/Fe interface as it is employed in technologically relevant devices. Thus, we are bridging the gap between structural studies of MgO/Fe interfaces on an atomic level and experiments that investigate TMR by transport measurements on the macroscopic scale.

VII. ACKNOWLEDGMENTS

The work was funded by the Land Nordrhein-Westfalen, the NRW Research School of Synchrotron Radiation. The beamtime at BESSY was funded by the BMBF (FK 05 ES3XBA/5). We thank the BESSY staff for their support. This work has also been supported by the Director, Office of Science, Office of Basic Energy Sciences, Materials Sciences and Engineering Division, of the U.S. Department of Energy under Contract No. DE-AC02-05CH11231, the Humboldt Foundation, and the Helmholtz Association.

---

[*] Electronic address: `sven.doering@tu-dortmund.de`

[1] P. Grünberg, D. Bürgler, H. Dassow, A. Rata, and C. Schneider, Acta Materialia **55**, 1171 (2007).

[2] T. Miyazaki and N. Tezuka, Journal of Magnetism and Magnetic Materials **139**, L231 (1995).

[3] J. S. Moodera, L. R. Kinder, T. M. Wong, and R. Meservey, Physical Review Letters **74**, 3273 (1995).

[4] S. A. Wolf, D. D. Awschalom, R. A. Buhrman, J. M. Daughton, S. von Molnar, M. L. Roukes, A. Y. Chtchelkanova, and D. M. Treger, Science **294**, 1488 (2001).

[5] S. D. Bader and S. S. P. Parkin, Annual Review of Condensed Matter Physics **1**, 71 (2010).

[6] Y. M. Lee, J. Hayakawa, S. Ikeda, F. Matsukura, and H. Ohno, Applied Physics Letters **90**, 212507 (2007).

[7] W. H. Butler, X.-G. Zhang, T. C. Schulthess, and J. M. MacLaren, Physical Review B **63**, 054416 (2001).

[8] J. Mathon and A. Umerski, Physical Review B **63**, 220403 (2001).

[9] S. Yuasa, T. Nagahama, A. Fukushima, Y. Suzuki, and K. Ando, Nature Materials **3**, 868 (2004).

[10] S. S. P. Parkin, C. Kaiser, A. Panchula, P. M. Rice, B. Hughes, M. Samant, and S.-H. Yang, Nature Materials **3**, 862 (2004).

[11] X. Feng, O. Bengone, M. Alouani, S. Lebègue, I. Rungger, and S. Sanvito, Physical Review B **79**, 174414 (2009).

[12] L. Plucinski, Y. Zhao, B. Sinkovic, and E. Vescovo, Physical Review B **75**, 214411 (2007).

[13] H. L. Meyerheim, R. Popescu, J. Kirschner, N. Jedrecy, M. Sauvage-Simkin, B. Heinrich, and R. Pinchaux, Physical Review Letters **87**, 076102 (2001).

[14] M. Müller, F. Matthes, and C. M. Schneider, EPL (Europhysics Letters) **80**, 17007 (2007).

[15] M. P. Seah and W. A. Dench, Surface and Interface Analysis **1**, 2 (1979).

[16] M. Gorgoi, S. Svensson, F. Schäfers, G. Öhrwall, M. Mertin, P. Bressler, O. Karis, H. Siegbahn, A. Sandell, H. Rensmo, et al., Nuclear Instruments and Methods in Physics Research Section A: Accelerators, Spectrometers, Detectors and Associated Equipment **601**, 48 (2009).

[17] S.-H. Yang, B. S. Mun, N. Mannella, S.-K. Kim, J. B. Kortright, J. H. Underwood, F. Salmassi, E. Arenholz, A. Young, Z. Hussain, et al., Journal of Physics: Condensed Matter **14**, L407 (2002).

[18] S.-H. Yang, B. S. Mun, A. W. Kay, S.-K. Kim, J. B. Kortright, J. H. Underwood, Z. Hussain, and C. S. Fadley, Journal of Electron Spectroscopy and Related Phenomena **114-116**, 1089 (2001).

[19] S.-H. Yang, B. S. Mun, and C. S. Fadley, Synchrotron Radiation News **17**, 23 (2004).

[20] S.-H. Yang, B. C. Sell, and C. S. Fadley, Journal of Applied Physics **103**, 07C519 (2008), invited.

[21] C. S. Fadley, S.-H. Yang, B. S. Mun, and J. G. de Abajo, *Solid-State Photoemission and Related Methods: Theory and Experiment* (Wiley-VCH Verlag, Berlin, 2003).

[22] S. Döring, F. Schönbohm, D. Weier, F. Lehmkühler, U. Berges, M. Tolan, C. S. Fadley, and C. Westphal, Journal of Applied Physics **106**, 124906 (2009).

[23] F. Schäfers, M. Mertin, and M. Gorgoi, Review of Scientific Instruments **78**, 123102 (2007).

[24] *X-ray interactions with matter*, URL `http://henke.lbl.gov/optical_constants/`.

[25] S.-H. Yang, B. S. Mun, N. Mannella, A. Nambu, B. C. Sell, S. B. Ritchey, F. Salmassi, A. Shick, S. S. P. Parkin, and C. S. Fadley, Journal of Physics: Condensed Matter **18**, L259 (2006).

[26] J. Zegenhagen, Surface Science Reports **18**, 199 (1993).

[27] S. Tanuma, C. J. Powell, and D. R. Penn, Surface and Interface Analysis **21**, 165 (1993).

[28] Y. Chen, F. J. García de Abajo, A. Chassé, R. X. Ynzunza, A. P. Kaduwela, M. A. Van Hove, and C. S. Fadley, Physical Review B **58**, 13121 (1998).